Available online at www.sciencedirect.com
SCIENCE DIRECT
Polymer 46 (2005) 7394–7402
polymer
www.elsevier.com/locate/polymer

Imprinting of nanopores in organosilicate dielectric thin films with hyperbranched ketalized polyglycidol

Jong-Seong Kim[1], Hyun-Chul Kim[1], Byeongdu Lee, Moonhor Ree*

Department of Chemistry, Center for Integrated Molecular Systems, School of Environmental Science and Engineering, Division of Molecular and Life Sciences and Polymer Research Institute, Pohang University of Science and Technology, San 31, Hyoja-dong, Pohang 790-784, South Korea

Received 28 November 2004; received in revised form 14 June 2005; accepted 14 June 2005
Available online 14 July 2005

Abstract

Hyperbranched polyglycidol (PG) was synthesized via a new polymerization pathway of glycidol using zinc glutarate (ZnGA) as a catalyst. ZnGA was found to be a highly active catalyst for the ring-opening polymerization of glycidol. The complex chemical structures of hyperbranched PG and its ketalized derivative (K-PG) were determined by specialized ^{13}C nuclear magnetic resonance spectroscopic techniques. In addition, a new soluble silsesquioxane copolymer, poly(methylsilsequioxane-*co*-1,4-bis(ethylsilsesquioxane)benzene), i.e. a PMSSQ–BESSQB precursor, was synthesized via the sol–gel reaction of its monomers. The precursor solution was found to produce good quality thin films. K-PG was found to have good solubility in common solvents and good miscibility with the PMSSQ–BESSQB precursor. Moreover, K-PG was found to exhibit a sacrificial thermal decomposition characteristic that makes it suitable for use as a porogen in the fabrication of porous PMSSQ–BESSQB dielectric films. K-PG can be loaded into the PMSSQ–BESSQB precursor at concentrations up to 40 wt%. Synchrotron grazing incident small-angle X-ray scattering studies of the porous thin films prepared from PMSSQ–BESSQB/K-PG composite films with various compositions found that the average size of pores in the porous dielectric films varies from 6.7 to 18.5 nm as the initial loading of the K-PG porogen is increased from 10 to 40 wt%. These pores are spherical and have a sharp interface with the dielectric matrix. The porosities *P* of the porous PMSSQ–BESSQB films were found to increase almost linearly from 0 to 37 vol% as the initial loading of the K-PG porogen was increased up to 40 wt%. The presence of the imprinted pores reduced the refractive index *n* and dielectric constant *k*values of the PMSSQ–BESSQB films almost linearly as the initial loading of the K-PG porogen was increased. These results lead to the conclusions that the sacrificial thermal decomposition of the K-PG porogen molecules successfully imprints nanopores into the PMSSQ–BESSQB dielectric films and that the population of the imprinted pores increases proportionally with increases in the initial loading of the porogen, up to concentrations of 40 wt%. The pore structures and properties of the nanoporous PMSSQ–BESSQB films imprinted by the K-PG porogen indicate that they are good candidates for use as interdielectric materials in the fabrication of advanced microelectronic devices.

Keywords: Nanoporous dielectric film; Low dielectric; Porogen

1. Introduction

The semiconductor and electronics industries have continued to reduce the size of integrated circuits (ICs) through the use of dense conductor-line wiring in multilevel structures and of smaller features, in order to increase device performance and to reduce costs [1,2]. However, smaller interconnect sizes lead to severe resistance–capacitance coupling problems including propagation delays and cross talk noise between interconnect conductors, which offset any speed advantage obtained from smaller device sizes [1,2]. To overcome these drawbacks of the reduction of the size of ICs, low dielectric constant (low-*k*) dielectrics are in high demand because they not only lower line-to-line noise in interconnect conductor lines, but also minimize power dissipation by reducing the capacitance between the interconnect conductor lines [1,2].

Much effort has, therefore, been exerted in the development of low-*k* dielectric materials, resulting in a variety of new dielectric materials [3–13]. Polyalkylsilsesquioxanes (PASSQs) have received much interest as an alternative to the workhorse dielectrics silicon dioxide

* Corresponding author. Tel.: +82 54 279 2120; fax: +82 54 279 3399.
E-mail address: ree@postech.edu (M. Ree).
[1] These authors contributed equally to this work.

0032-3861/$ - see front matter © 2005 Elsevier Ltd. All rights reserved.
doi:10.1016/j.polymer.2005.06.024

($k=3.9$–4.3) and silicon nitride ($k=6.0$–7.0) because of their relatively low k values ($k=2.7$–3.3), low moisture uptake, high breakdown voltage, and high mechanical and thermal stability, in addition to the ease of spin-coating their soluble precursors [3–13]. In particular, polyhydrogensilsesquioxane (PHSSQ) and polymethylsilsesquioxane (PMSSQ) have been extensively investigated as representative PASSQs, but improvements are still needed in their mechanical properties, including their crack-resistance [3–13]. The k values of PASSQs are nevertheless much higher than the lowest attainable k ($=1.0$), that of air (or vacuum). There has thus been much interest in incorporating voids into dielectric materials in order to produce porous materials with low k values (≤ 2.5) [3–5,12–23].

One promising approach is templating nanoporosity into thin films of PASSQ dielectrics using thermally labile organic porogens [3–5,12,13,15–23]. The porogens have to decompose completely in a small temperature range within the 200–400 °C region, in which PASSQ precursors favorably undergo a curing reaction, creating nanopores [12,13,15–23]. Several porogen systems have been reported thus far: Linear random and block copolymers [15–18], and star-shaped polymers [12,13,19,20–22]. These porogens exhibit thermal degradation below 400 °C that is well-matched with the vitrification temperature range of PASSQ precursors [12,13,15–22]. However, these porogens have been found to exhibit phase separation and aggregation in PASSQ precursor matrices, which limit the pore size reduction and the porosity of the resulting dielectric thin films [12,13,15–22]. In the case of star-shaped porogens, a higher number of arms was found to produce severe segregation and aggregation even at 10 wt% porogen loading, which results in large and interconnected pores in the dielectric thin films [12,13,19–22]. Hyperbranched organic polymers are another type of thermally labile porogen. Hyperbranched polymer porogens have only rarely been studied to date, in comparison to the many studies of the linear random and block copolymers and star-shaped polymers described above. Hyperbranched poly(ε-caprolactone) is the only hyperbranched porogen introduced so far [20,24]. This hyperbranched polymer has better miscibility with PMSSQ precursor matrices than star-shaped poly(ε-caprolactone) porogens, but there are limits on its loading into PMSSQ precursor matrices and on the reductions in pore size [20–22,24]. Therefore, the challenge remains to develop new porogens that have better miscibility with dielectric matrices and that enable higher porosity and smaller size pores in the resulting dielectric matrices.

In this study, a hyperbranched polyether, polyglycidol (PG), was synthesized via a novel route for the polymerization of glycidol using zinc glutarate catalyst, and then its shell structure was chemically modified by ketalization. The chemical structure of ketalized polyglycidol (K-PG) was characterized in detail using the inverse gated (IG) and distortionless enhancement by polarization transfer (DEPT) carbon nuclear magnetic resonance (^{13}C NMR) spectroscopic techniques. In addition, the PMSSQ–BESSQB precursor poly(methylsilsequioxane-*co*-1,4-bis(ethylsilsesquioxane)benzene) was synthesized from methyltrimethoxysilane and bis(1,2-trimethoxysilylethyl) benzene. Nanoporous dielectric thin films were prepared by the templated polymerization of PMSSQ–BESSQB precursor (the dielectric matrix) in the presence of K-PG (the porogen) and subsequent calcination of the porogen at 400 °C, then characterized by spectroscopic ellipsometry and synchrotron small-angle X-ray scattering.

2. Experimental

2.1. Materials and synthesis

Methyltrimethoxymethylsilane and bis(trimethoxysilylethyl)benzene were purchased from Gelest, Inc. and used without further purification. All other chemicals and reagents were purchased from Aldrich Chemical Company and used as received. Zinc glutarate (ZnGA) was synthesized from zinc oxide and glutaric acid in accordance with a method described previously [25–31].

The polymerization of glycidol was carried out in an autoclave equipped with a mechanical stirrer (Scheme 1). Prior to polymerization, the autoclave containing the ZnGA catalyst (0.5 g) was dried in vacuum at 100 °C for 10 h and cooled to 70 °C. After glycidol (50 mL) was added to the autoclave, polymerization proceeded for 10 h at 70 °C. The polymerization product was dissolved in distilled water and the precipitated catalyst was then filtered out. The filtrate was concentrated and dried for 24 h at 120 °C in vacuum. The polyglycidol (PG) product was obtained as a pale brown, highly viscous liquid in a yield of 85%. The ketalization of polyglycidol with dimethylacetal was performed using *p*-toluenesulfonic acid (PTSA) as a catalyst (Scheme 1), according to a procedure described in the literature [32].

Soluble PMSSQ–BESSQB precursor was prepared by carrying out the sol–gel reaction of methyltrimethoxysilane (MTMOS, 90 mol%) and bis(1,2-trimethoxysilylethyl)benzene (BTMSEB, 10 mol%) as follows (Scheme 2). MTMOS (6.0 g, 44 mmol) and BTMSEB (1.83 g, 49 mmol) were added to a flame-dried flask containing tetrahydrofuran (THF, 18.7 g). With rapid stirring, distilled water (1.40 g, $[H_2O]/[MTMOS]=1.7$) was slowly dropped into the monomer mixture. After addition, the mixture was stirred at room temperature for an additional 10 min. HCl (0.15 g, $[HCl]/[MTMOS]=0.03$) was slowly added to the reaction mixture, which was then stirred at room temperature for 1 h. After the room temperature reaction, the reaction mixture was heated to 60 °C and stirred for an additional 12 h at that temperature. After the reaction was complete, the remaining acid was extracted several times with distilled water. The product solution was dried with anhydrous magnesium sulfate. The solvent was then removed from the product by rotary evaporation. The resulting viscous liquid was washed

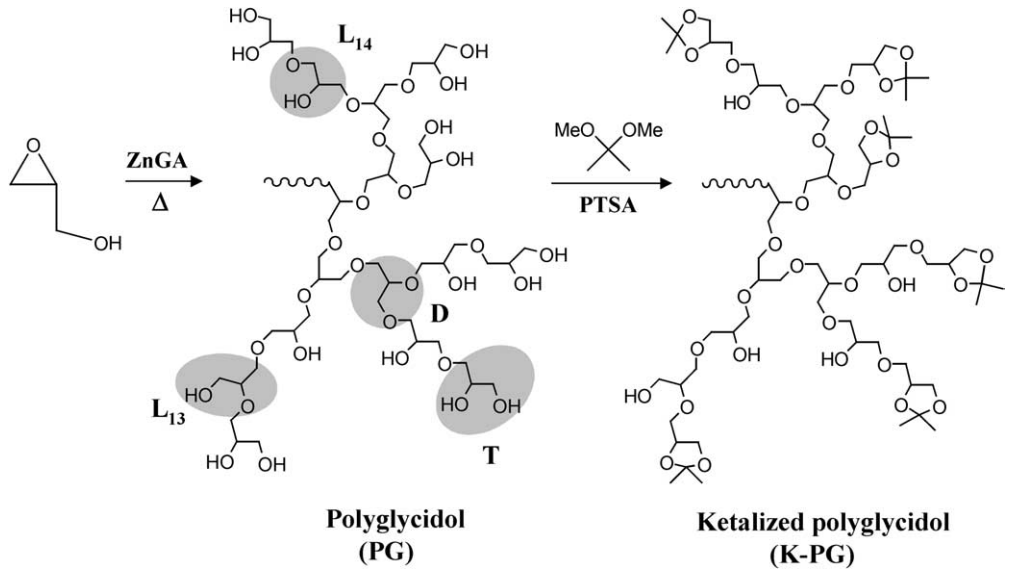

Scheme 1. Scheme for synthesis of hyperbranched polyglycidol (PG) from glycidol using a new zinc glutarate (ZnGA) catalyst and for ketalization of its hydroxyl terminal groups; PTSA is *p*-toluenesulfonic acid. The terminal (T), dendritic (D), linear 1,3- (L_{13}), and linear 1,4-units (L_{14}) in the PG are marked by shading.

with *n*-pentane to remove low molecular weight product, and then finally dried in vacuum for 3 h at room temperature, giving the precursor product as a white powder.

2.2. Film preparation

A series of homogeneous solutions of the hyperbranched K-PG porogen and the PMSSQ–BESSQB precursor in 1,2-propanediol monomethyl ether acetate (PMEAc) (10.0 wt% solid) were prepared using porogen compositions of 10, 20, 30 and 40 wt% (Scheme 3). Each solution was filtered using a PTFE-membrane filter of pore size 0.20 μm, spin-coated onto precleaned Si(100) wafers, and then dried at 50 °C for 1 h under a nitrogen atmosphere. The dried samples were heat-treated up to 400 °C at a rate of 2.0 °C/min under a nitrogen atmosphere and held at that temperature for 1 h, before slow cooling to room temperature (Scheme 3).

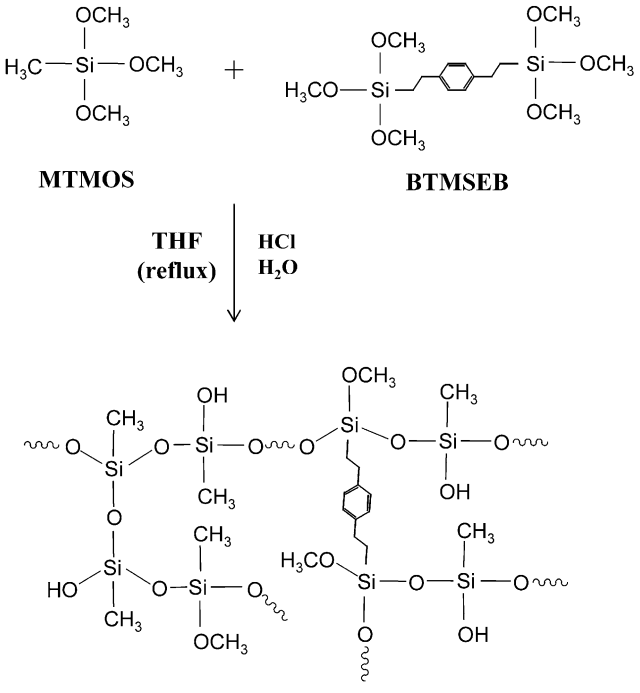

Scheme 2. Scheme for synthesis of poly(methylsilsequioxane-*co*-1,4-bis(ethylsilsesquioxane)benzene), PMSSQ–BESSQB precursor, from methyltrimethoxysilane (MTMOS) and bis(1,2-trimethoxysilylethyl)benzene (BTMSEB).

2.3. Measurements

Proton and carbon nuclear magnetic resonance (^{1}H and ^{13}C NMR) spectra were recorded on a Bruker Aspect 300 spectrometer, using dimethyl-d_6 sulfoxide (DMSO-d_6) as the internal reference. Weight-average molecular weight ($\bar{M}_w$) and polydispersity index (PDI) measurements were carried out with a gel permeation chromatography (GPC) system (Wyatt Technology) calibrated with polystyrene standards and using THF as an eluent. Thermogravimetry analysis (TGA) was carried out under a nitrogen atmosphere using a Perkin–Elmer thermogravimeter (Model TGA-7). The flow rate of nitrogen gas was 80 mL/min and the heating rate was 2.0 °C/min. Ellipsometric measurements were carried out using a spectroscopic ellipsometer (VASE, J.A. Woollam) equipped with a Xe lamp light source. Grazing incident small-angle X-ray scattering (GISAXS) measurements were conducted at the 4C1 Beamline of the Pohang Accelerator Laboratory [33]. The energy of X-rays from a bending magnet was monochromatized to 7.25 keV and a charge-coupled detector (CCD, Princeton Instruments) was used. A sample to detector distance of about 2845 mm was chosen. Each sample was mounted on a *z*-axis goniometer equipped with a vacuum chamber. Aluminium

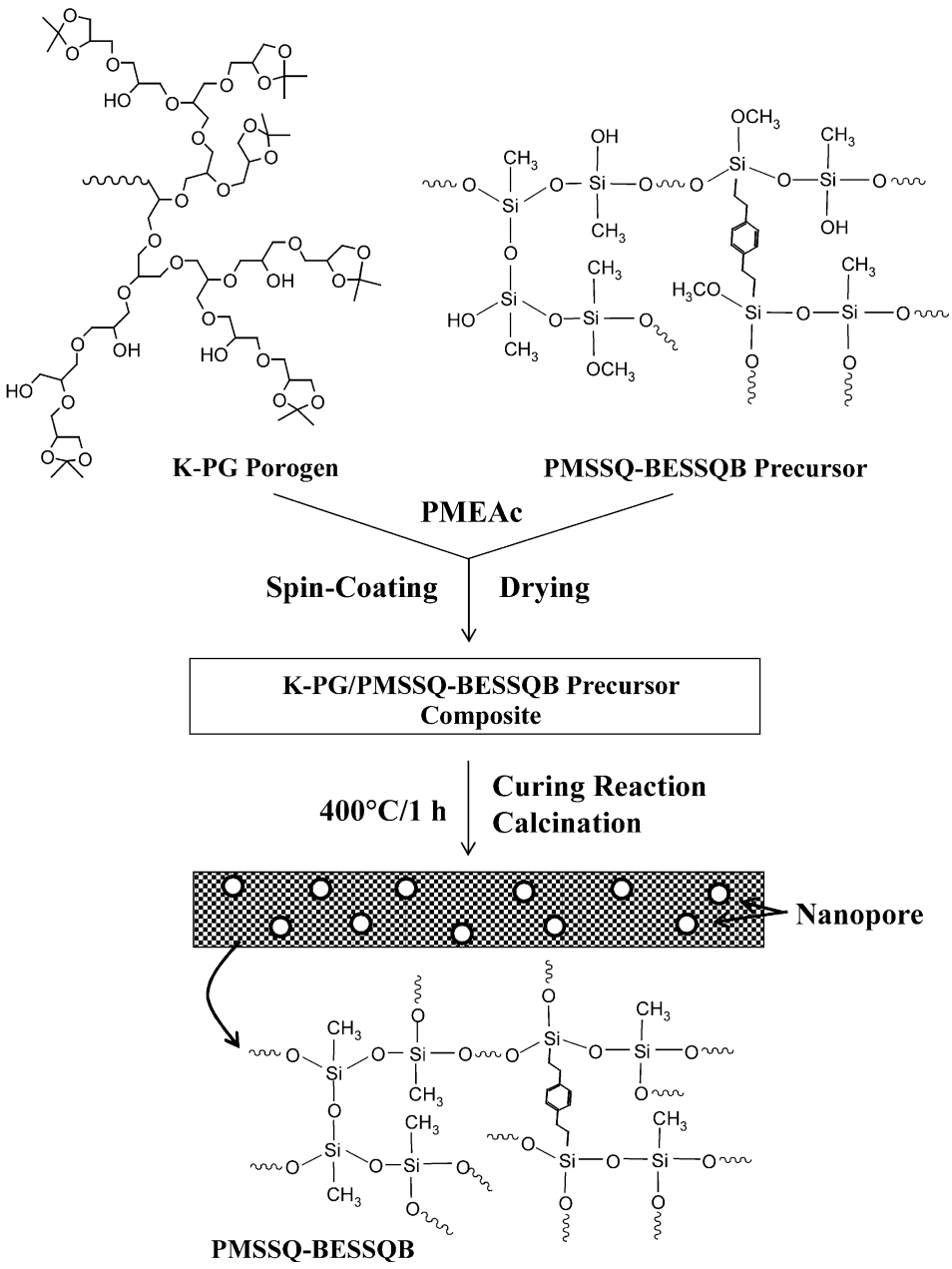

Scheme 3. Preparation scheme for nanoporous poly(methylsilsequioxane-*co*-1,4-bis(ethylsilsesquioxane)benzene) (PMSSQ–BESSQB) dielectric thin films imprinted with hyperbranched ketalized polyglycidol (K-PG); PMEAc: 1,2-propanediol monomethyl ether acetate.

foil strips were employed as semi-transparent beam stops. Scattering angles were corrected by precalibrated block copolymer standards. Each GISAXS pattern was typically collected for 100 s at an incidence angle between the critical angles of the dielectric film and the Si wafer [12,13]. Data were typically collected for 100 s.

3. Results and discussion

3.1. Synthesis

It is known that ZnGA catalyzes the copolymerization of carbon dioxide with oxiranes such as propylene oxide [22–28]. NEXAFS studies have found that ZnGA reacts facilely with propylene oxide as a result of the chemical absorption of propylene oxide onto the ZnGA surface [31]. In this study, we attempted to extend the use of ZnGA as a catalyst to the ring-opening polymerization of glycidol. The two unsymmetrically structured reactive sites (i.e. cyclic ethers (or hydroxyl groups when the ring has been opened) and hydroxyl groups) of glycidol may lead in its ZnGA-catalyzed ring-opening polymerization to a complex hyperbranched structure that is composed of four different structural units: Dendritic (D), 1,3-(L_{13}) and 1,4-linear (L_{14}), and terminal (T) units (Scheme 1). The synthesized

PG products were characterized in detail using several NMR spectroscopy techniques in order to determine their structures.

Fig. 1 shows typical ^{1}H, IG ^{13}C, and DEPT ^{13}C NMR spectra of the hyperbranched PG products. As can be seen in Fig. 2(b) and (c), hyperbranched PG produces seven peaks in the range 60–90 ppm. With the aid of previously reported results [32,34,35], the carbon peaks in Fig. 1(b) and (c) were assigned as follows: (i) L_{13} unit (Scheme 1): CH_2OH at 61.7 ppm, CH_2 at 70.5 ppm, and CH at 80.5 ppm; (ii) L_{14} unit: CH_2 at 73.5 ppm, and $CHOH$ at 69.2 ppm; (iii) T unit: CH_2OH at 63.9 ppm, $CHOH$ at 71.3, and CH_2 at 71.6 ppm; (iv) D unit: CH at 78.5 ppm, and CH_2 72.4 ppm. These results indicate that the PG product that results from the ZnGA-catalyzed polymerization of glycidol is a hyperbranched polyether consisting of four different branching units.

Fig. 1(a) shows a ^{1}H NMR spectrum of PG in which the methylene and methine protons produce overlapping broad peaks in the range 3.41–3.82 ppm and the signal due to hydroxyl protons is split into three peaks between 4.61 and 4.91 ppm. These proton peaks can be assigned by taking the above ^{13}C NMR data into account: The proton peak at 4.63 ppm corresponds to the hydroxyl group of the L_{13} unit, that at 4.78 ppm to the hydroxyl group of the T unit, and that at 4.91 ppm to the hydroxyl group of the L_{14} unit.

By using the above carbon peak assignments, the IG ^{13}C spectrum in Fig. 1(b) can be interpreted to determine the relative populations of the four different structural units. From the integrations of the carbon peaks in Fig. 1(b), the PG product was found to be composed of 14.2% D units, 13.6% L_{13} units, 36.7% L_{14} units, and 35.5% T units. From these relative populations, the degree of branching (DB) of the PG product was estimated to be 0.3 using the following relationship [35]:

$$\mathrm{DB} = \frac{2D}{2D + L_{13} + L_{14}} \quad (1)$$

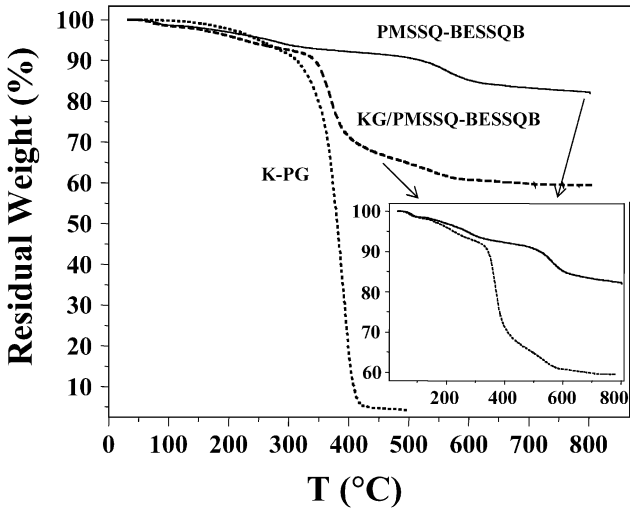

Fig. 2. Thermogravimetric diagrams for K-PG, PMSSQ–BESSQB precursor, and their composite (80 wt% PMSSQ–BESSQB precursor and 20 wt% K-PG); Inset: Magnified thermogravimetric diagrams of PMSSQ–BESSQB precursor and its composite with K-PG (20 wt%). All thermogravimetric measurements were conducted at 2.0 °C/min under a nitrogen atmosphere.

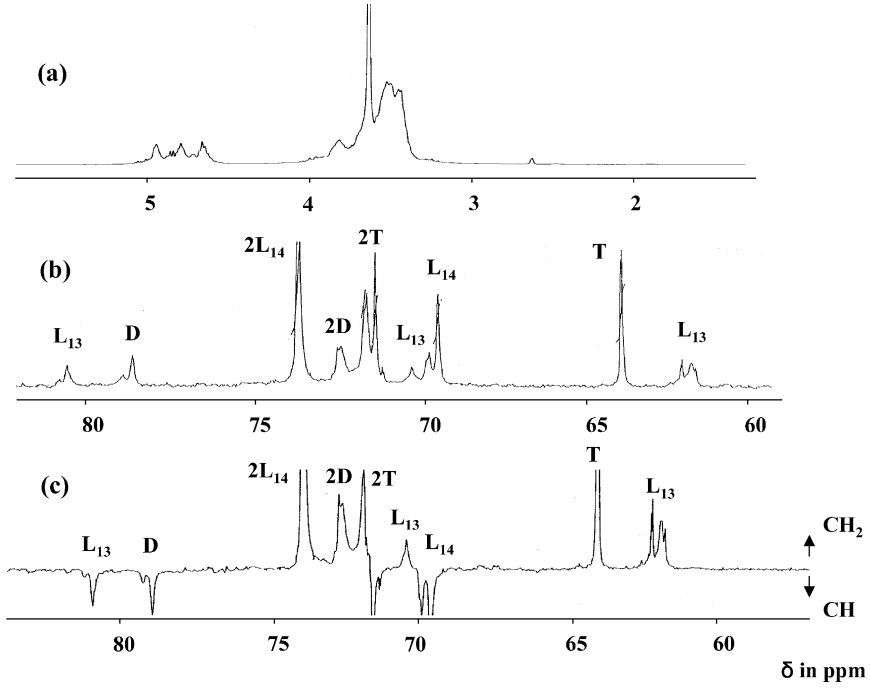

Fig. 1. Nuclear magnetic resonance (NMR) spectra of polyglycidol obtained from the zinc glutarate-catalyzed ring-opening polymerization of glycidol: (a) ^{1}H NMR spectrum; (b) inverse gated (IG) ^{13}C NMR spectrum; (c) DEPT ^{13}C NMR spectrum. The terminal, dendritic, linear 1,3- and linear 1,4-units are represented by T, D, L_{13} and L_{14}, respectively, as shown in Scheme 1.

In general, DB = 0 for a fully linear structure and DB = 1 for a fully dendritic structure. DB = 0.30 suggests that the PG product is a hyperbranched polymer with a structure that is intermediate between a fully linear and a fully dendritic structure. However, this DB value is much lower than that (DB = 0.5–0.6) reported for PG materials synthesized using metal alkoxide catalysts [35]. The low DB value of this study suggests that the ZnGA catalyst has better affinity and selectivity with one of the two reactive sites of glycidol monomer in the ring-opening polymerization, than is observed with the conventional metal alkoxide catalysts. According to previous studies [25–31], the active site of the ZnGA catalyst is the Zn(II) metal center with its Lewis acid characteristics, which reacts readily with propylene oxide via its adsorption onto the catalyst surface and insertion into the Zn–O bond. On the other hand, in the glycidol monomer the cyclic ether oxygen atom is more Lewis basic than the hydroxyl oxygen atom. Thus the Lewis acidic Zn(II) metal center is likely to have more affinity with the cyclic ether group than with the hydroxyl group in the glycidol monomer. Therefore it is expected that the ZnGA-catalyzed polymerization takes place via the adsorption and insertion of the cyclic ether oxygen atoms of glycidol into the Zn–O bonds of the ZnGA catalyst, rather than via the adsorption and insertion of both the reactive oxygen atoms of glycidol into the Zn–O bonds of the ZnGA catalyst, which results in a lower DB valued PG product.

The resulting PG material was found to exhibit good solubility in water but very poor solubility in other solvents including most common organic solvents. Due to its poor solubility, its molecular weight was not successfully determined in GPC measurements. To improve the solubility, the ketalization of the PG material was performed with dimethylacetal and *p*-toluenesulfonic acid monohydrate as described previously [32], giving ketalized polyglycidol (K-PG) (Scheme 1). The K-PG was found to exhibit good solubility, which made it possible to determine its molecular weight analysis using GPC. The K-PG was determined to have a weight-average molecular weight ($\bar{M}_w$) of 5200 with a polydispersity index (PDI) of 4.0.

In addition to the synthesis of PG and K-PG, a new soluble silsesquioxane copolymer, PMSSQ–BESSQB precursor, was synthesized via the sol–gel reaction of MTMOS (90 mol%) and BTMSEB (10 mol%) in THF using hydrochloric acid and water as catalysts (Scheme 2). The resulting PMSSQ–BESSQB precursor was found to have a $\bar{M}_w$ of 4200 and a PDI of 1.84. Solutions of this precursor were found to produce good quality thin films through conventional spin-casting, drying and curing processes.

3.2. Thermal properties

To investigate the usefulness of K-PG as a porogen (i.e. pore generator) in PMSSQ–BESSQB dielectric films, the thermal degradation behavior of hyperbranched K-PG was studied by TGA under nitrogen with a heating rate of 2.0 °C/min and then compared with that of the PMSSQ–BESSQB precursor and of their composite.

Fig. 2 shows the weight variation of the dried K-PG porogen with temperature, as measured during the heating run. At first, the weight of the K-PG sample drops very slowly with increasing temperature up to approximately 305 °C, which is due to the removal of residual solvent. The weight then drops rapidly with further increases in the temperature, which is due to thermal degradation. The K-PG completely decomposes near 420 °C.

The dried PMSSQ–BESSQB precursor exhibits the following weight loss behavior (Fig. 2) during heating runs at 2.0 °C/min under a nitrogen gas atmosphere: Its weight drops as the temperature is increased up to approximately 305 °C and then decreases more slowly with further increase of the temperature up to 520 °C. Above this temperature, the weight drops rapidly with increasing temperature. The secondary polycondensation (i.e. curing reaction) of the PMSSQ precursor is known to occur in the temperature range between room temperature and 300 °C, producing water and alkyl alcohol (methanol or ethanol, depending on the alkoxy group of its starting silane monomer) as by-products [6–10]. Thus the observed weight losses between 25 and 305 °C are attributed to the evaporation of the residual solvent and of the by-products (water, ethanol, and methanol) that result from the secondary polycondensation (i.e. the curing reaction) of the precursor. The relatively large weight losses above 520 °C are due to thermal degradation of the cured PMSSQ–BESSQB polymer. Thus the weight losses in the 305–520 °C region are attributed to the evaporation of the by-products of the continuous curing reaction of the precursor, which is not complete after the heating from room temperature to 305 °C during the heating run.

The weight loss behaviors of the K-PG porogen and the PMSSQ–BESSQB precursor can be used to explain the weight loss behaviors of their composites. A typical weight loss behavior of a composite is shown in Fig. 2, which was obtained for a PMSSQ–BESSQB precursor composite loaded with 20 wt% K-PG. At first, the weight of the composite drops slowly with increasing temperature up to approximately 350 °C, which is mainly due to the evaporation of the by-products (water, ethanol, and methanol) of the curing reaction of the precursor component, as well as of residual solvent. The weight then drops steeply with further increases in temperature until 400 °C is reached, and this decline is mainly due to the thermal decomposition of the K-PG component and also partly due to the removal of by-products of the continuing curing reaction. Above this temperature the weight slowly decreases with temperature up to 520 °C, which is due to the removal of the K-PG residue, as well as of any further by-products of the curing reaction. Above 520 °C, the cured PMSSQ–BESSQB component begins to decompose. The onset decomposition temperature of the K-PG component of the composite is 350 °C, which is 45 °C higher than that of

K-PG, but the final decomposition temperature of K-PG in the composite is the same as that of K-PG. This result indicates that the porogen becomes more stable in the PMSSQ–BESSQB matrix, which is attributed to a kinetic barrier to its decomposition produced by the matrix.

These TGA results show that during the heating run, first the PMSSQ–BESSQB precursor vitrifies through its curing reaction below 305 °C, even in the presence of the hyperbranched K-PG molecules, and thereafter the K-PG molecules undergo sacrificial thermal degradation in a relatively narrow temperature range (350–400 °C), generating pores in the PMSSQ–BESSQB dielectric that has been dimensionally stabilized by the prior curing reaction. We conclude that the hyperbranched K-PG is a good porogen for the PMSSQ–BESSQB precursor.

3.3. Optical and dielectric properties

A series of porous thin films prepared from PMSSQ–BESSQB/K-PG composite films with various compositions were investigated using spectroscopic ellipsometry, according to a method reported previously [13,36]. From the measured refractive indices (n), dielectric constants k were estimated using the simple Maxwell–Garnett equation, $k = n^2$ [37]. The results are summarized in Table 1 and Fig. 3.

As can be seen in Table 1, the cured PMSSQ–BESSQB films exhibit $n = 1.45$ and $k = 2.1$ at 630 nm wavelength, which are higher than those ($n = 1.388$ and $k = 1.926$) of PMSSQ films cured under the same conditions [12,13]. These results indicate that the introduction of a diethylphenyl moiety between the two trimethoxy silanes makes the organosilicate films denser than the PMSSQ films. The n and k values of the cured PMSSQ–BESSQB films decrease almost linearly as the initial loading of the K-PG porogen is increased up to 40 wt% (Fig. 3 and Table 1).

The relative porosities P of the porous PMSSQ–BESSQB dielectric films with respect to the cured PMSSQ–BESSQB dielectric films were estimated from their refractive indices using the Lorentz–Lorenz relationship [38,39]:

$$\frac{n_0^2 - 1}{n_0^2 + 2}(1 - P) = \frac{n^2 - 1}{n^2 + 2} \quad (2)$$

where n_0 is the refractive index of the cured PMSSQ–BESSQB film without any porogen loading and n is the refractive index of a porous PMSSQ–BESSQB film prepared with an initial loading of the K-PG porogen. The results are summarized in Fig. 3 and Table 1; it can be seen that the porosities of the porous PMSSQ–BESSQB films increase almost linearly as the initial loading of the K-PG porogen is increased up to 40 wt% (Fig. 3 and Table 1).

Table 1
Pore structures and properties of nanoporous PMSSQ–BESSQB dielectric thin films imprinted with hyperbranched K-PG porogen

Porogen content (%)	Average pore size (nm)[a]	Refractive index (n)[b]	Porosity (vol%)[c]	Dielectric constant (k)[d]
0	–	1.45	–	2.10
10	6.7	1.39	12	1.93
20	7.5	1.37	16	1.88
30	10.8	1.30	30	1.69
40	18.5	1.27	37	1.61

[a] Average pore size determined from the log–log plot of the GISAXS profile.
[b] Refractive index at 630 nm was measured using spectroscopic ellipsometry.
[c] Porosity was estimated from the measured refractive indices using the Lorentz–Lorenz relationship [38,39].
[d] Dielectric constant was estimated from the measured refractive index using the Maxwell–Garnett equation ($k = n^2$) [37].

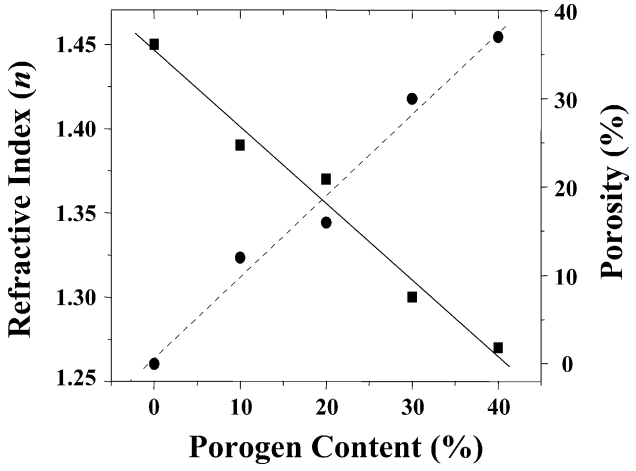

Fig. 3. Refractive indices and porosities of nanoporous PMSSQ–BESSQB dielectric films imprinted with varying K-PG porogen loadings. The refractive indices at 630 nm were measured using spectroscopic ellipsometry, and the porosities were estimated from the measured refractive indices using the Maxwell–Garnett equation ($k = n^2$) [34].

These results indicate that the sacrificial thermal decomposition of the K-PG porogen molecules successfully imprints pores in the PMSSQ–BESSQB dielectric films and that the population of imprinted pores increases proportionally to the initial loading of the porogen for concentrations up to 40 wt%. Moreover, it is worth noting that the upper limit (i.e. 40 wt%) for loading of the K-PG porogen into the PMSSQ–BESSQB precursor is higher than that (30 wt%) for the loading of hyperbranched poly(ε-caprolactone) into PMSSQ precursor, which is the only previously reported hyperbranched porogen [20,24].

3.4. Structure

The porous PMSSQ–BESSQB dielectric films were further characterized using the GISAXS technique with synchrotron radiation sources in order to determine their structures. Two-dimensional (2D) GISAXS patterns were measured at an incidence angle of 0.3°, i.e. between the critical angles of the dielectric film and the Si wafer. GISAXS profiles were extracted from the 2D GISAXS

patterns along the horizontal direction at an exit angle of 0.22°. The extracted GISAXS profiles are displayed in Fig. 4.

As can be seen in this figure, the intensity of the GISAXS profile in the low angle region increases as the initial loading of the K-PG porogen increases, which is attributed to an increase in the volume fraction of pores as the initial loading of the porogen increases. On the other hand, the GISAXS profiles are found at high angle regions to vary with q^{-4}, which is characteristic of X-ray scattering from hard spheres; $q=(4\pi/\lambda)\sin\theta$ (i.e. the magnitude of scattering vector) where 2θ is the scattering angle and λ is the wavelength of the X-ray beam. These results imply that pores generated in the PMSSQ–BESSQB dielectric have a spherical rather than a random shape, and also that the pores have a sharp interface with the dielectric matrix.

The size of pores was determined as π/q^* from the downturn point q^* in the log–log plot of the GISAXS profiles (q^* marked in Fig. 4), according to a previously reported method [18]. The pore sizes are summarized in Table 1. As can be seen in this table, the average pore size varies from 6.7 to 18.5 nm as the initial loading of the K-PG porogen increases from 10 to 40 wt%. We attempted to fit the GISAXS profiles with the Pedersen formulae [40] by assuming spherical pores in monomodal distributions such as Gaussian and log-normal [18], but were unsuccessful. This suggests that the nanopores in the PMSSQ–BESSQB dielectric films have a broad pore size distribution, which might be due to the aggregation of some porogen molecules during the porous film forming process. However, the pores produced in this study are still smaller than those in porous PMSSQ dielectric films templated by hyperbranched poly(ε-caprolactone) [20,24] and by star-shaped poly(ε-caprolactone)s [12,13,19–22]. Moreover, the pores in the nanoporous dielectric films of this study are much smaller than the sizes of the features of advanced integrated circuits.

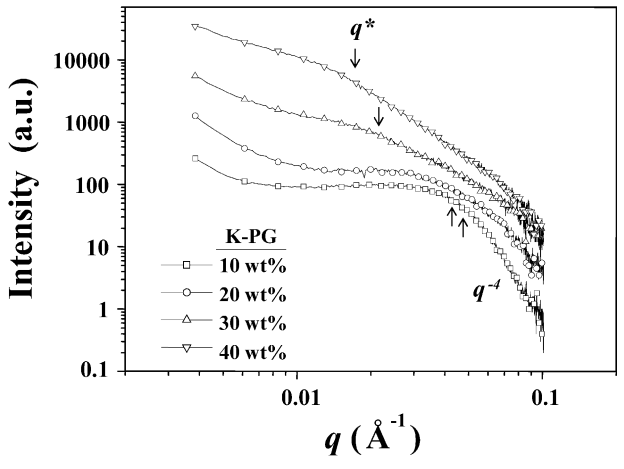

Fig. 4. GISAXS profiles of porous PMSSQ–BTMSEB films extracted from the measured two-dimensional (2D) GISAXS patterns along the horizontal direction at an exit angle of 0.22°. The marked arrow on each GISAXS profile indicates the downturn point q^* in the log–log plot of the GISAXS profile. Above q^*, the log–log plots of the GISAXS profiles follow a q^{-4} power law.

4. Conclusions

A new soluble silsesquioxane copolymer, PMSSQ–BESSQB precursor, was synthesized via the sol–gel reaction of its monomers in THF using hydrochloric acid and water as catalysts. The precursor solution was found to produce good quality thin films through conventional spin-cast, drying and curing processes. Cured PMSSQ–BESSQB films were found to exhibit $n=1.45$ and $k=2.1$ at 630 nm, which are higher than those ($n=1.388$ and $k=1.926$) of conventional PMSSQ films. The relatively large n and k values of the PMSSQ–BESSQB dielectric are due to the higher density that results from the presence of the covalent diethylphenyl linkers.

Hyperbranched PG was successfully synthesized via the ZnGA-catalyzed ring-opening polymerization of glycidol, which is a new polymerization pathway for glycidol. ZnGA was found to be a highly active catalyst for the ring-opening polymerization of glycidol. The complex chemical structure of hyperbranched PG was successfully determined using IG ^{13}C and DEPT ^{13}C NMR as well as ^{1}H NMR spectroscopy. The ketalization of the hydroxyl terminal groups in PG improved its solubility in common solvents and also its miscibility with the PMSSQ–BESSQB dielectric precursor. The ketalized PG (K-PG) was found to exhibit thermal decomposition behavior over a narrow temperature of 350–400 °C, which is higher than the temperature range in which the curing of the PMSSQ–BESSQB dielectric precursor takes place but is still far below the thermal degradation temperature of the cured dielectric. Thus K-PG has thermal decomposition characteristics that make it suitable for use as a porogen in the sacrificial formation of porous PMSSQ–BESSQB dielectric films. It was found that K-PG could be loaded into the PMSSQ–BESSQB precursor at concentrations up to 40 wt%. The upper limit (i.e. 40 wt%) for loading of the K-PG porogen into the PMSSQ–BESSQB precursor is higher than that (30 wt%) for the previously reported hyperbranched poly(ε-caprolactone) porogen for use in PMSSQ precursor [20–22,24].

A series of porous thin films were successfully prepared from PMSSQ–BESSQB/K-PG composite films with various compositions. GISAXS studies of these dielectric films found that the average size of pores in the porous dielectric films varies from 6.7 to 18.5 nm as the initial loading of the K-PG porogen is increased from 10 to 40 wt%. These pores are spherical with a sharp interface with the dielectric matrix. The size distribution of pores is broad due to some degree of aggregation of the porogen molecules that occurs during the porous film formation process and this broadness increases as the initial loading of the porogen increases. However the pores created in this study are still smaller than those of porous PMSSQ dielectric films templated with

hyperbranched poly(ε-caprolactone) [20,24] or star-shaped poly(ε-caprolactone)s [12,13,19–22]. Moreover, the pores in the nanoporous dielectric films of this study are much smaller than the sizes of the features of advanced integrated circuits. In addition, the porosities *P* of the porous PMSSQ–BESSQB films were found to increase almost linearly from 0 to 37 vol% as the initial loading of the K-PG porogen was increased up to 40 wt%. Due to the contribution of the imprinted pores, the *n* and *k* values of the PMSSQ–BESSQB films were found to decrease almost linearly as the initial loading of the K-PG porogen was increased.

We conclude that the K-PG porogen molecules were successfully used to imprint nanopores in PMSSQ–BESSQB dielectric films though their sacrificial thermal decomposition and that the population of the imprinted pores increases proportionally to the initial loading of the porogen for increases in the concentration of up to 40 wt%. These pore structures and properties make nanoporous PMSSQ–BESSQB films imprinted with the K-PG porogen good candidates for use as interdielectric materials in the fabrication of advanced microelectronic devices.

Acknowledgements

This study was supported by MIE and MOST (contracted under M103BY010035-03B2501-03550), and by KOSEF (CIMS). Synchrotron GISAXS measurements were supported by MOST and POSCO.

References

[1] The international technology roadmap for semiconductors. Austin, TX: International SEMATECH; 2002.
[2] Czornyj G, Chen KJ, Prada-Silva G, Arnold A, Souleotis H, Kim S, et al. Proc Elect Comp Tech (IEEE) 1992;42:682.
[3] Maiser G. Prog Polym Sci 2001;26:3.
[4] Morgan M, Ryan ET, Zhao J-H, Hu C, Cho T, Ho PS. Annu Rev Mater Sci 2000;30:645.
[5] Miller RD. Science 1999;286:421.
[6] Baney RH, Itoh M, Sakakibara A, Suzuki T. Chem Rev 1995;95:1409.
[7] Brinker CJ. Sol–gel science: The physics and chemistry of sol–gel processing. San Diego: Academic Press; 1990.
[8] Oh W, Shin TJ, Ree M, Jin MY, Char K. Macromol Chem Phys 2002; 203:791.
[9] Oh W, Ree M. Langmuir 2004;20:6932.
[10] Lee J-K, Char K, Rhee H-W, Ro HW, Yoo DY, Yoon D. Polymer 2001;42:9085.
[11] Lu Y, Fan H, Doke N, Loy DA, Assink RA, LaVan DA, et al. J Am Chem Soc 2000;122:5258.
[12] Bolze J, Ree M, Youn HS, Chu S-H, Char K. Langmuir 2001;17:6683.
[13] Oh W, Hwang Y-T, Park YH, Ree M, Chu S-H, Char K, et al. Polymer 2003;44:2519.
[14] Ree M, Goh WH, Kim Y. Polym Bull 1995;35:215.
[15] Lee H-J, Lin EK, Wang H, Wu W-L, Chen W, Moyer EC. Chem Mater 2002;14:1845.
[16] Yang S, Mirau PA, Pai C-S, Nalamasu O, Reichmanis E, Lin EK, et al. Chem Mater 2001;13:2762.
[17] Kim H-C, Volksen W, Miller RD, Huang E, Yang G, Briber RM, et al. Chem Mater 2003;15:609.
[18] Huang E, Toney MF, Volksen W, Mecerreyes D, Brock P, Kim H-C, et al. Appl Phys Lett 2002;81:2232.
[19] Nguyen CV, Carter KR, Hawker CJ, Hedrick JL, Jaffe RL, Miller RD, et al. Chem Mater 1999;11:3080.
[20] Hedrick JL, Miller RD, Hawker CJ, Carter KR, Volksen W, Yoon DY, et al. Adv Mater 1998;10:1049.
[21] Lee B, Yoon J, Oh W, Hwang Y, Heo K, Jin KS, et al. Macromolecules 2005;39:3395.
[22] Lee B, Oh W, Hwang Y, Park Y-H, Yoon J, Jin KS, et al. Adv Mater 2005;17:696.
[23] Lee B, Park Y-H, Hwang Y-T, Oh W, Yoon J, Ree M. Nat Mater 2005;4:147.
[24] Nguyen C, Hawker CJ, Miller RD, Huang E, Hedrick JL. Macromolecules 2000;33:4281.
[25] Hwang Y-T, Jung J, Ree M, Kim H. Macromolecules 2003;36:8210.
[26] Ree M, Bae JY, Jung JH, Shin TJ. J Polym Sci Polym Chem 1999;37: 1863.
[27] Ree M, Bae JY, Jung JH, Shin TJ, Hwang Y-T, Chang T. Polym Eng Sci 2000;40:1542.
[28] Ree M, Bae JY, Jung JH, Shin TJ. Korea Polym J 1999;7:333.
[29] Ree M, Bae JY, Jung JH, Shin TJ, Hwang Y-T, Chang T. Polym Eng Sci 2000;40:1542.
[30] Kim J-S, Ree M, Shin TJ, Han OH, Cho SJ, Hwang Y-T, et al. J Catal 2003;218:209.
[31] Kim J-S, Ree M, Lee SW, Hwang Y-T, Baek S, Lee B, et al. J Catal 2003;218:386.
[32] Haag R, Stumbe J-F, Sunder A, Frey H, Hebel A. Macromolecules 2000;33:8158.
[33] Bolze J, Kim J, Lee B, Shin TJ, Huang J-Y, Rah SG, et al. Macromol Res 2002;10:2.
[34] Dworak A, Walach W, Trzebicka B. Macromol Chem Phys 1995;196: 1963.
[35] Sunder A, Hanselmann R, Frey H, Mulhaupt R. Macromolecules 1999;32:4240.
[36] Tompkins HG, McGahan WA. Spectroscopic ellipsometry and reflectometry. New York: Wiley; 1999.
[37] Maxwell-Garnett JC. Philos Trans Royal Soc London 1905;205:237.
[38] Lorentz HA. Ann Phys Chem 1880;9:641.
[39] Lorentz L. Ann Phys Chem 1880;11:70.
[40] Pedersen JS. J Appl Cryst 1994;27:595.